School of Natural Sciences and Mathematics

On the Origin of Ionospheric Hiss: A Conjugate Observation

UT Dallas Author(s):

Lunjin Chen

Citation:

Zhima, Zeren, Lunjin Chen, Ying Xiong, Jinbin Cao, et al. 2017. "On the origin of Ionospheric hiss: A conjugate observation." Journal of Geophysical Research—Space Physics 122(11): 11784-11793, doi:10.1002/2017JA024803

AGU PUBLICATIONS

JGR

Journal of Geophysical Research: Space Physics

RESEARCH ARTICLE

10.1002/2017JA024803

On the Origin of Ionospheric Hiss: A Conjugate Observation

Zeren Zhima[1], Lunjin Chen[2], Ying Xiong[3,4], Jinbin Cao[5], and Huishan Fu[5]

[1]Institute of Earthquake Science, China Earthquake Administration, Beijing, China, [2]Department of Physics, University of Texas at Dallas, Richardson, TX, USA, [3]Institute of Space Physics and Applied Technology, Peking University, Beijing, China, [4]PKU/UCLA Joint Research Institute in Science and Engineering, Peking University, Beijing, China, [5]Space Science Institute, School of Astronautics, Beihang University, Beijing, China

Key Points:
- A conjugate observation reveals that the ionospheric and plasmaspheric hiss share similar time-frequency structures and spectral properties
- Ray tracing simulations indicate that the connection between ionospheric and plasmaspheric hiss is physically possible
- This study suggests that the downward plasmaspheric hiss is one generation source for ionospheric hiss

Correspondence to:
Z. Zhima,
zrzm@seis.ac.cn

Citation:
Zhima, Z., Chen, L., Xiong, Y., Cao, J., & Fu, H. (2017). On the origin of ionospheric hiss: A conjugate observation. *Journal of Geophysical Research: Space Physics*, *122*, 11,784–11,793. https://doi.org/10.1002/2017JA024803

Received 21 SEP 2017
Accepted 9 NOV 2017
Accepted article online 13 NOV 2017
Published online 24 NOV 2017

Abstract We present a conjugate observation on whistler mode electromagnetic hiss from the low Earth orbit satellite Detection of Electro-Magnetic Emissions Transmitted from Earthquake Regions (DEMETER) and the high-altitude elliptical orbit spacecraft Time History of Events and Macroscale Interactions during Substorms (THEMIS). The conjugate observation was performed at 14:51:10 to 15:12:00 UT on 15 June 2010, when DEMETER was flying across the L shell region from ~1.39 to 2.80 at an altitude of ~660 km; meanwhile, THEMIS probes were passing through the L shell region from ~1.64 to 1.91 at altitudes from ~1.6 to 2.0 R_E. The conjugated observations demonstrate similar time-frequency structures between the ionospheric hiss (~350 to 800 Hz) captured by DEMETER and the plasmaspheric hiss (~350 to 900 Hz) recorded by THEMIS probes, including similar peak frequencies (~500 to 600 Hz), similar lower cutoff frequencies (~350 to 400 Hz), and upper cutoff frequencies (~730 to 800 Hz). The wave vector analyses show that the ionospheric hiss propagates obliquely downward to the Earth and slightly equatorward with right-handed polarization, suggesting that its source comes from higher altitudes. Ray tracing simulations with the constraint of observations verify that the connection between ionospheric and plasmaspheric hiss is physically possible through wave propagation. This study provides direct observational evidence to support the mechanism that high-altitude plasmaspheric hiss is responsible for the generation of low-altitude ionospheric hiss.

1. Introduction

Hiss is a broadband structureless whistler mode electromagnetic emission at extremely low frequency range from ~100 Hz to 3 kHz (Bortnik et al., 2009; Thorne et al., 1973), and it predominates in a cold dense plasma region from the upper ionosphere to a region about ~3 R_E in the inner magnetosphere, namely, plasmasphere (Bortnik et al., 2008; Fu et al., 2010). Hiss plays a vital role in either the loss of energetic electrons (Breneman et al., 2015; Chen, Thorne, et al., 2012) or the formation of radiation belt slot region (Meredith, Horne, Glauert, et al., 2006; Thorne, 2010).

Hiss in the high-altitude plasmasphere (or the inner magnetosphere), widely known as plasmaspheric hiss (Thorne et al., 1973), has received more attention than that in low-altitude region, especially in the upper ionosphere. However, recent studies suggest that hiss in the upper ionosphere region (named ionospheric hiss in this paper) is a promising tool to study wave propagation mechanism and ionosphere-magnetosphere interaction, for it might be a manifestation of the downward magnetospheric emission. Ray tracing simulations (Bortnik et al., 2009, 2008; Chen, Bortnik, et al., 2012; Chen et al., 2017) reveal that a certain fraction of whistler mode magnetospheric emissions can avoid magnetospheric reflection when the wave frequency is below the local lower hybrid resonant frequency. Instead of propagating toward higher latitude, it leaks into plasmasphere and subsequently merges as incoherent unstructured plasmaspheric hiss (Bortnik et al., 2011, 2009). Some of the leaked fractions can even reach down to the upper ionosphere region, serving as a source of ionospheric hiss before collisional damping becomes significant (Chen et al., 2017).

Observations from the low Earth orbit satellite DEMETER provide evidence for the downward magnetospheric emission source. DEMETER's observations demonstrate that ionospheric hiss (Parrot et al., 2014; Santolík, Němec, et al., 2006; Zhima et al., 2014) generally exhibits similar broadband incoherent unstructured features to those typical plasmaspheric hiss waves (Bortnik et al., 2009, 2008; Thorne et al., 1973). Ionospheric hiss generally appears over frequencies from ~100 Hz to 1 kHz (Němec et al., 2013; Parrot, Buzzi, et al., 2006; Santolík, Chum, et al., 2006; Santolík, Němec, et al., 2006) and mainly predominates at dayside and high-latitude ionosphere (Zhima et al., 2014). During some storms, ionospheric hiss can also exhibit chorus-like discrete spectra (Parrot, Buzzi, et al., 2006; Parrot et al., 2016; Santolík, Chum, et al., 2006) or quasiperiodic

structures (Hayosh et al., 2013; Němec et al., 2013). DEMETER even captured an intense storm event of whistler mode chorus penetrating the plasmapause and entering into high-latitude ionosphere (Zhima et al., 2013). In short, previous studies based on DEMETER's observations suggest that ionospheric hiss resembles the downward magnetospheric whistler mode emissions, which propagate from the inner magnetosphere, and support the idea that ionospheric hiss might originate from the downward whistler mode emissions.

The downward magnetospheric emission includes chorus and plasmaspheric hiss. The downward chorus is widely considered as a possible source for the ionospheric hiss (Parrot, Benoist, et al., 2006; Parrot, Buzzi, et al., 2006; Parrot et al., 2016; Santolík, Chum, et al., 2006; Santolík, Němec, et al., 2006), and the plasmapheric hiss is another source (if not a major source) recently proposed by Chen et al. (2017). The generation mechanism of the downward magnetospheric emission for ionospheric hiss has recently received increasing attention because it explains most of the features seen in the ionosphere with frequencies from ~100 Hz to 1 kHz. However, the conjugated observation connecting magnetospheric emissions to the ionospheric emission has yet to be verified directly due to the lack of satellite constellation simultaneously operating in both the ionosphere and magnetosphere.

Fortunately, there was a 2 year overlapped period (2009 to 2010) between the low Earth orbit satellite DEMETER and the high-altitude elliptical orbit spacecraft THEMIS, which occasionally operate at close conjugate configurations. We define the conjugate criterion (shown later) to identify a conjugate event and then investigate whether similar whistler mode emissions are observed at conjugate points. In this paper, we present a rare conjugate event according to a thorough investigation over the overlapped period between DEMETER and THEMIS. Detailed analyses indicate that the observed ionospheric hiss and plasmaspheric hiss are parts of the same emission. Ray tracing simulations with the constraint of observations confirm that the plasmaspheric hiss wave is indeed the source of the ionospheric hiss.

2. Data and the Conjugate Event

DEMETER was operating at a Sun-synchronous circular orbit (10:30 and 22:30 LT) at an altitude from 710 km (before December 2015) to 660 km (Parrot, Benoist, et al., 2006) over a 6 year period from November 2004 to December 2010. The electromagnetic observations of DEMETER satellite are obtained from the electric field experiment (ICE) (Berthelier et al., 2006) and the search-coil magnetometer (IMSC) (Parrot, Benoist, et al., 2006). The electron density and temperature are derived from the Langmuir probe (ISL) (Lebreton et., 2006).

THEMIS spacecraft launched in 2007 with five probes is still in operation. Measurements from THEMIS probe A (THA), probe D (THD), and probe E (THE) are used in this study. These probes are located in the inner magnetosphere following a highly elliptical and near-equatorial orbits with a perigee ~1.5 R_E and apogee ~12 R_E (Angelopoulos, 2008). The observations from the Fluxgate Magnetometer (FGM) (Auster et al., 2008), the Search Coil Magnetometer (SCM) (Roux et al., 2008), the Electric Field Instrument (EFI) (Bonnell et al., 2008), and the particle Electrostatic Analyzer (ESA) (McFadden et al., 2008) on board THEMIS probes are used in this study.

We compared foot point locations of satellites at the same universal time (UT) to identify conjugate positions between DEMETER and THEMIS probes. The geomagnetic main field model IGRF combined with the external magnetic field T96 model (Tsyganenko & Stern, 1996) are adopted to compute foot point locations, which are obtained in terms of L shell, magnetic latitude (MLAT), and magnetic local time (MLT). We defined a conjugate criterion based on their foot point locations: $|\Delta L_{fp}| \leq 1$ and $|\Delta \mathrm{MLT}_{fp}| \leq 2$ h, where ΔL_{fp} is L shell difference of foot points and$\Delta \mathrm{MLT}_{fp}$ is MLT difference of foot points. A conjugate event is established when the foot point difference between DEMETER and at least one of THEMIS probes satisfies the conjugate criterion. Then we examined the specific electromagnetic observations for those identified conjugate events to check whether the same type of whistler mode emissions appeared at conjugate points by analyzing wave spectral properties. Among the 144 conjugate events from 2009 to 2010, only 1 event on 15 June 2010 captured both ionospheric and plasmaspheric hiss at conjugate positions of DEMETER and THEMIS probes.

The satellite locations, projected onto a meridian plane during this event, are illustrated in Figure 1. The red, magenta, blue, and green lines represent orbits of DEMETER, THA, THD, and THE, respectively. The conjugate

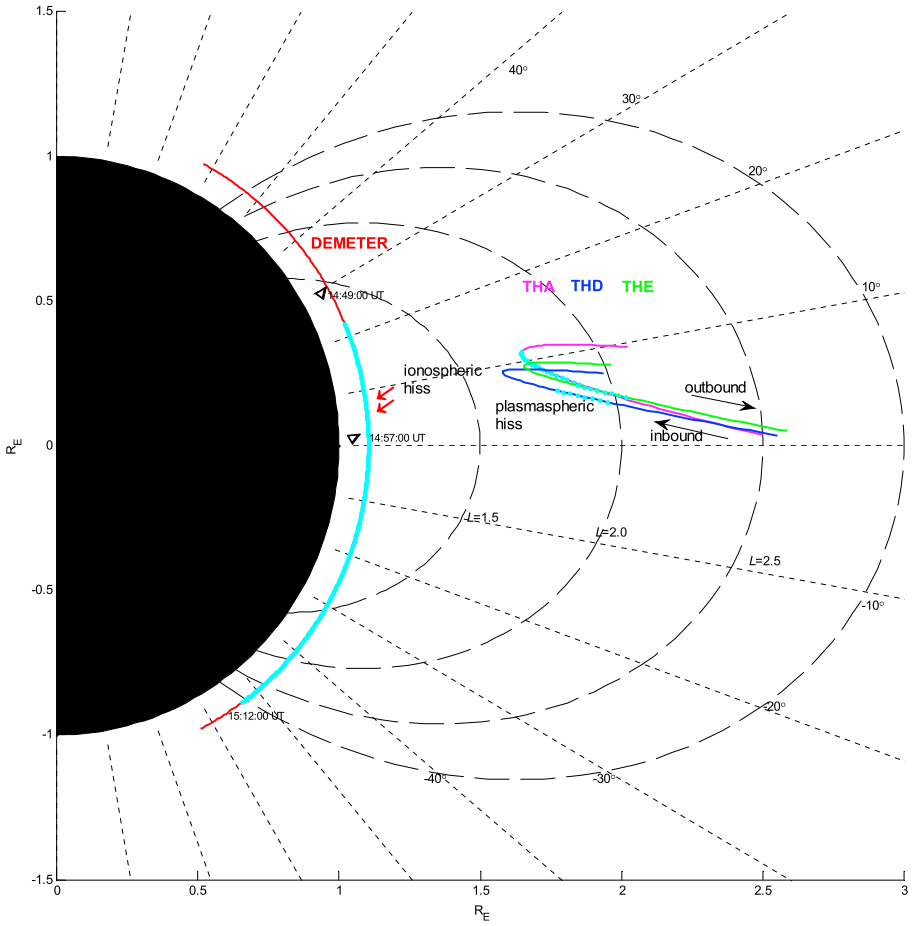

Figure 1. The meridian projection of satellite orbits on 15 June 2010. Orbit traces highlighted in cyan denote the conjugate period. Triangles display DEMETER's burst mode observation triggered from 14:49 to 14:57 UT. Red arrows schematically show propagation direction of the ionospheric hiss. Radial dotted lines display the constant magnetic latitude lines and dashed curves denote the *L* shells.

observation between DEMETER and THA took place from 14:51:10 to 15:12:00 UT, lasting about 21 min (orbit traces highlighted in cyan). When DEMETER was passing from the Northern Hemisphere (MLAT ~ 22.47°, L ~ 1.39 at 14:51:10 UT) to the Southern Hemisphere (MLAT ~ −54.3°, L ~ 2.8 at 15:12:00 UT) at a low altitude of ~ 660 km, and THA was flying outbound from the L shell region ~1.75 to 1.91 (1.69 to 1.88 R_E). Then the conjugate observation among DEMETER, THD, and THE occurred at 15:06:05 to 15:11:55 UT (see

Table 1
Orbital Details of DEMETER and THEMIS Probes During the Conjugate Event on 15 June 2010

Satellites	Conjugate time	*Orbit L* shell	Orbit MLT (h)
DEMETER versus THA	14:51:10 UT to 15:12:00 UT	DEMETER: 1.39 to 2.80 THA: 1.75 to 1.91 Min (Δ*L*): 0.06 Max(Δ*L*): 0.9	DEMETER: 9.57 to 8.89 THA: 7.58 to 10.86 Min(ΔMLT): 0.02 Max(ΔMLT):1.99
DEMETER versus THD	15:06:05 UT to 15:11:55 UT	DEMETER: 1.59 to 2.41 THD: 1. 66 to 1.64 Min (Δ*L*): 0.06 Max(Δ*L*): *0.78*	DEMETER: 9.14 to 8.96 THD: 7.30 to 8.06 Min(ΔMLT): 0.89 Max(ΔMLT): 1.83
DEMETER versus THE	15:06:10 UT to 15:11:55 UT	DEMETER: 1.59 to 2.41 THE: 1. 74 to 1.72 Min(Δ*L*): 0.0 Max(Δ*L*): *0.69*	DEMETER: 9.14 to 8.96 THE: 7.18 to 8.87 Min(ΔMLT): 1.08 Max(ΔMLT): 1.96

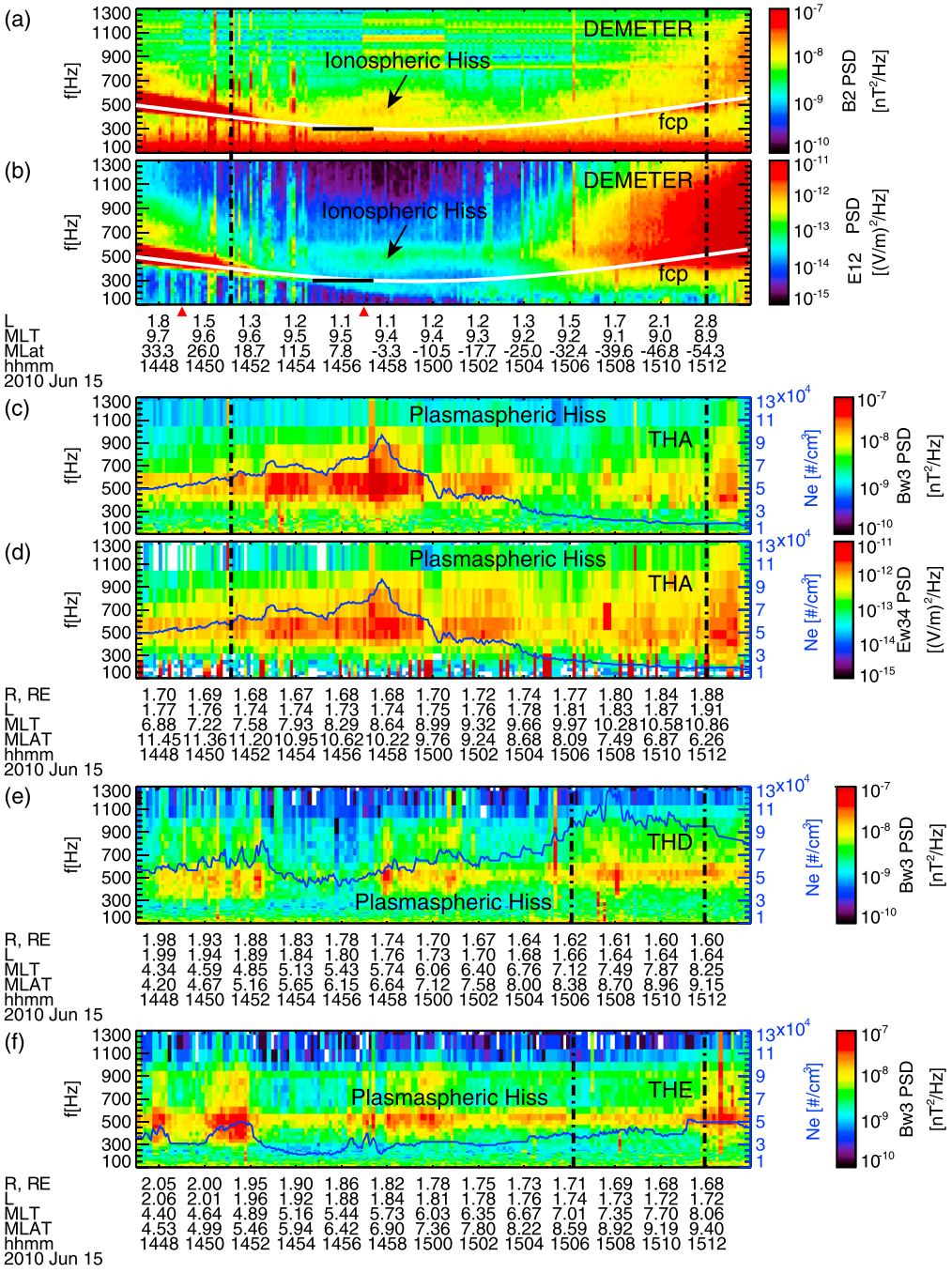

Figure 2. Overview of electromagnetic observations during the conjugate event. Wave spectra represented by power spectral density (PSD) values. (a, b) DEMETER's observation of the magnetic *B2* component and electric *E12* component in sensor coordinate; (c, d) THA's observations of the magnetic *Bw3* component and electric *Ew34* component; (e) THD's observations of the magnetic *Bw3* component; and (f) THE's observations at the magnetic *Bw3* component. The vertical dashed lines represent the conjugate period between DEMETER and THEMIS probes; the two red triangles in Figures 2a and 2b denote burst mode observations; the overlapped curves in Figures 2c–2f represent electron density. The data displayed as a function of universal time UT (hhmm), magnetic latitude (MLAT/degree), magnetic local time (MLT/hour), and *L* shell.

cyan parts of blue and green colored orbits), when THD was flying inbound from the *L* shell region ~1.66 to 1.64 (1.62 to 1.60 R_E), and THE was also flying inbound from the *L* shell region ~1.74 to 1.72 (1.71 to 1.68 R_E), respectively. The detailed satellite orbit (not foot point) information during this conjugate event is listed in

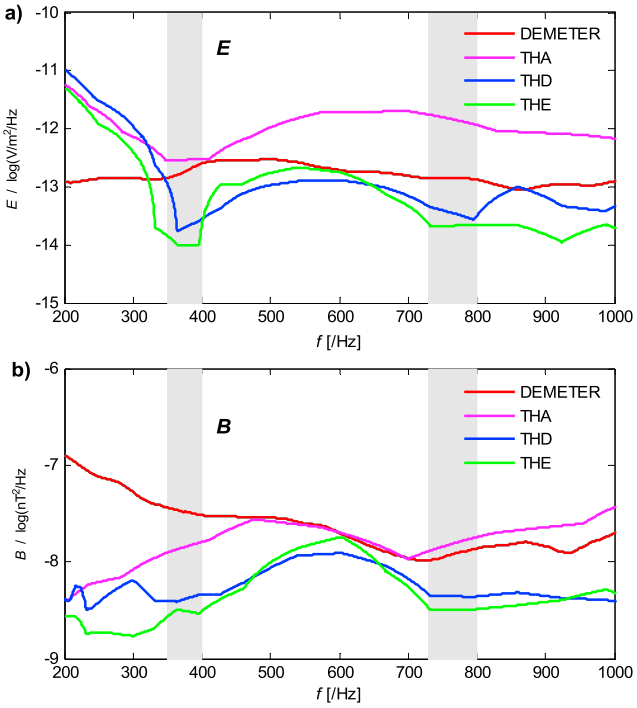

Figure 3. Comparison of wave structures between the ionospheric and plasmaspheric hiss observed at 14:59 UT. (a) PSD values of electric components and (b) PSD values of magnetic components.

Table 1. The spectral properties of the observed ionospheric and plasmaspheric hiss are analyzed, and their relationships are discussed in the following sections.

3. Observations

Figure 2 shows an overview of electromagnetic measurements by DEMETER and THEMIS probes during the conjugate event on 15 June 2010. The vertical dashed lines represent the exact conjugate periods for DEMETER and THEMIS probes.

Figures 2a and 2b show the ionospheric hiss recorded by DEMETER. The power spectral density (PSD) of the magnetic *B2* component recorded by IMSC and electric *E12* component measured by ICE in sensor coordinate show that ionospheric hiss waves appear as narrowband spectra from ~ 350 to 800 Hz above the proton cyclotron frequency f_{cp} (as shown in Figures 2a and 2b). Wave intensities of the ionospheric hiss mainly peak at a frequency range from ~500 to 600 Hz.

Plasmaspheric hiss emissions recorded by THEMIS probes are displayed in Figures 2c–2f. The overlapped blue curves represent the observed electron density obtained from ESA instrument. Figures 2c and 2d show THA's measurement at the magnetic *Bw3* component (along spin axis direction, recorded by SCM) and electric *Ew34* component (recorded by EFI). In Figures 2c and 2d, the plasmaspheric hiss mainly appears at a frequency range from ~350 to 900 Hz, and wave intensities mainly peak at a frequency band from ~500 to 600 Hz. THD and THE's measurements of magnetic *Bw3* components are shown in Figures 2e and 2f. The electric observations are not shown since their spectral features are similar to those of the magnetic components. Compared with hiss waves recorded by THA, one can see that THD and THE also recorded structured waves over similar frequency ranges, frequency peaks, and with comparable intensities. Considering that THEMIS probes were operating within a very narrow *L* shell region, from ~1.64 to 1.91 (see Table 1), we suggest that these emissions are the same plasmaspheric hiss event.

A further comparison of wave structures between the observed ionospheric and plasmaspheric hiss over the same time intervals reveals similar time-frequency structures at remote locations. See one of the results at 14:59:00 UT in Figure 3, showing wave power spectral density of the electric and magnetic components. In Figure 3, the observed ionospheric and plasmaspheric hiss have similar structures: lower cutoff frequencies near ~380 to 400 Hz, upper cutoff frequencies near ~730 to 800 Hz (denoted as gray shadows), and wave intensity peak near ~500 to 600 Hz. Note that DEMETER's relatively high magnetic field intensity over the frequency range 200 to 350 Hz is due to artificial noises most likely from the satellite platform or payload (see Figure 2a).

Considering the conjugate relations between DEMETER and THEMIS locations, we conclude that the observed ionospheric and plasmaspheric hiss are the same event. To support this conclusion further, high-resolution waveform data are required to compute wave propagation characteristics. Fortunately, DEMETER performed burst mode observations with a sampling frequency of 2.5 kHz from 14:49 to 14:57 UT (marked by two triangles, respectively, in Figure 1 and Figures 2a and 2b), providing 2 min of waveform data from 14:55 to 14:57 UT (highlighted by two thick horizontal lines in Figures 2a and 2b) for the ionospheric hiss relevant to our study.

We adopted DEMETER's local geomagnetic coordinate system, where the *Z* axis directs along the total magnetic field B_0 and the *X* axis lies in the magnetic meridian plane and points away from the Earth, to compute wave propagation parameters during the period from 14:55 to 14:57 UT. The angles θ_k and ϕ_k are defined as the wave normal angle (polar angle) and the azimuthal angle between the total magnetic field B_0 and the wave vector *k*. The angles θ_s and ϕ_s are defined as the polar angle and azimuthal angle between the total magnetic field B_0 and Poynting flux vector *S*. Under this coordinate system, a value of 180° in azimuthal

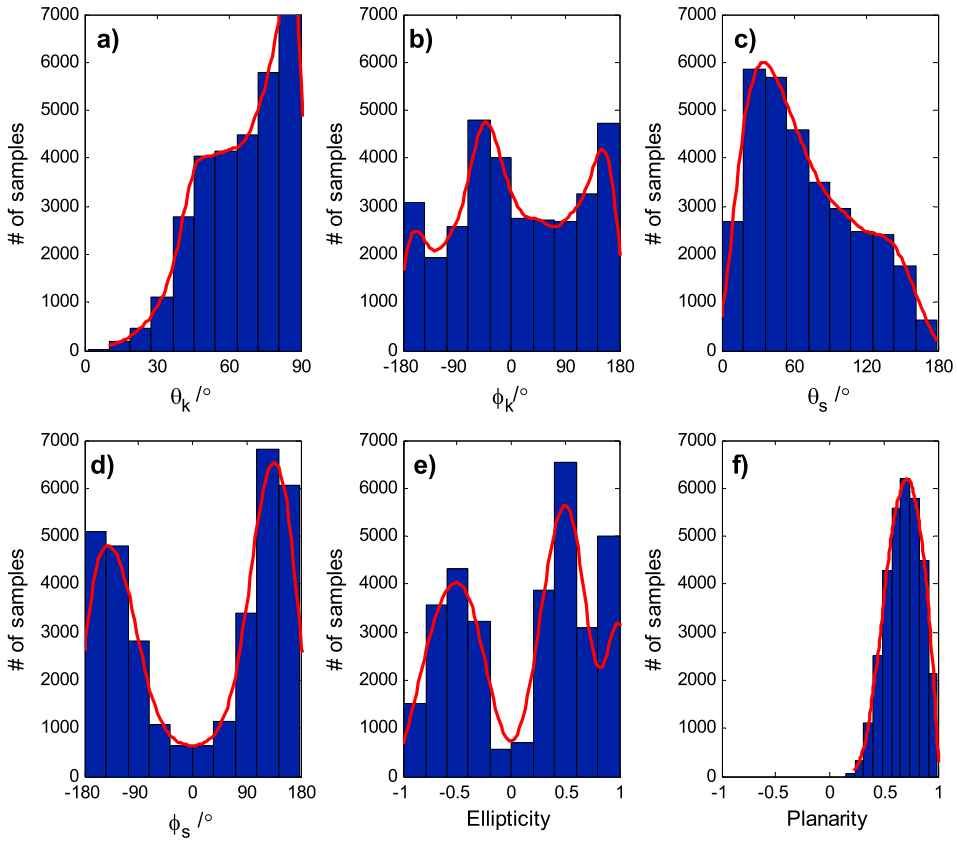

Figure 4. Distribution of wave propagation parameters of ionospheric hiss computed from burst mode waveform at 14:55 to 14:57 UT. The overlapped red lines represent fitted curves computed by a probability density function; (a, b) wave normal angle θ_k and azimuth angle ϕ_k of the wave vector, (c, d) the polar angle θ_s and the azimuth angle ϕ_s of Poynting flux *S*, (e) ellipticity, and (f) planarity.

angle ϕ_k and ϕ_s represents that the wave vector *k* and Poynting flux vector *S* propagate toward the Earth direction (decreasing *L* shell), while 0° means the opposite direction (increasing *L* shell) in the meridian plane.

We used the wave vector analysis singular value decomposition method (Santolík et al., 2003) to compute wave propagation parameters at a frequency range from 350 to 800 Hz for the ionospheric hiss. The statistical distributions of wave propagation parameters θ_k, ϕ_k, θ_s, and ϕ_s are shown in Figures 4a and 4b. The overlapped red curves represent the fitted curves computed by the kernel density distribution function (Rudemo, 1982). The majority of wave normal angles θ_k are in the range from 50° to 85°, and the azimuthal angles ϕ_k exhibit as three peaks: ±160° and −40°. For Poynting flux vector *S*, polar angles θ_s mostly range from ~30° to 60°, and the azimuthal angles ϕ_s mainly predominate around ±150°.

The polarization feature is described by ellipticity and planartiy in Figures 4e and 4f. It can be seen that the planarity is about 0.8 to 1 (Figure 2f), suggesting that the ionospheric hiss waves are polarized nearly in a single plane (Santolík et al., 2003). For ellipticity representing the ratio of the axes of polarization ellipse, a value of +1 means the right-handed circular polarization, −1 represents left-handed, and 0 corrresponds to linear polarization (Santolík et al., 2003). Figure 4e shows that the majority of the electromagnetic hiss demonstrates ellipticity values over 0.5 to 1, indicating that the observed hiss is roughly right-hand polarized. To further confirm polarization feature of the ionospheric hiss, we filtered the waveform at its peak frequencies (~500 to 600 Hz) to compute the polarization by using the minimum variance analysis (MVA) put forward by Sonnerup and Scheible (1998). We computed the time series of magnetic field vectors in the MVA coordinate system over the different time intervals between 14:55 and 14:57 UT, and results confirm that polarization of the ionospheric hiss at the peak frequencies is indeed right handed. Figure 5 shows one of the results at 14:56:45.000 to 14:56:45.080 UT. Panels from left to right in Figure 5 represent the degree of polarization of the magnetic field in the MVA coordinate system, that is, three components along the

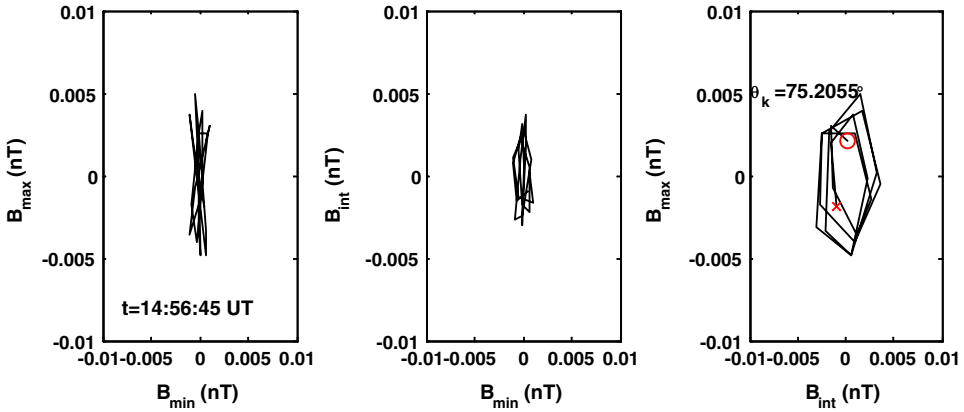

Figure 5. Polarization of the ionospheric hiss at its peak frequencies (~500 to 600 Hz) at 14:56:45 UT, computed by minimum variance analysis (MVA). The circle and cross represent the start and end of the time series, respectively.

directions of maximum variance, intermediate variance and minimum variance. The time series of magnetic field vectors in Figure 5 indicate that the observed ionospheric hiss is indeed right-hand polarized.

In all, the above wave vector analyses indicate that the major portion of the observed ionospheric hiss obliquely propagate downward to the Earth and slightly toward the equatorial region with right-handed polarization. The propagation direction is schematically denoted by red arrows in Figure 1.

The intense emissions with broadband spectra at high-latitude ionosphere (MLAT: ~30° to ~60°) at both the Northern and Southern Hemisphere are hiss, too (Chen et al., 2017), which are very common in the upper ionosphere (Parrot et al., 2016; Santolík, Chum, et al., 2006; Zhima et al., 2013). For this type of high-latitude ionospheric hiss, a burst mode waveform from 14:49 to 14:52 UT was used to examine the wave propagation parameters. The distribution of wave propagation parameters (not shown) indicates that the majority of wave normal angles θ_k present at ~60° to 90° and azimuthal angles ϕ_k are around 180°. Polar angles θ_s of Poynting flux are mostly around 100°, and azimuthal angles ϕ_s are mainly around 180°. This suggests that a major portion of these high-latitude ionospheric hiss propagate obliquely downward to the Earth, indicating that these high-latitude ionospheric hiss also propagate downward from high-altitude regions.

The above analyses imply that the observed ionospheric hiss most likely originate from the plasmaspheric hiss. Unfortunately, there are no burst mode waveform data available from the THEMIS probes. Therefore, we simulated wave propagation process from THEMIS to DEMETER by means of a ray tracing code for electromagnetic waves in magnetized plasma medium.

4. Discussions

To confirm the conjecture that the observed ionospheric hiss may originate from the plasmaspheric hiss, we performed a ray tracing simulation to examine the propagation path of plasmaspheric hiss in a magnetized plasma medium with constraints of the present observation. The ray tracing is done in a 2-D meridian plane by using the HOTRAY code, a well-established ray tracing code for waves in magnetized plasma medium (Horne, 1989).

A dipole magnetic field model is adopted in the HOTRAY code, and a modified diffusive equilibrium model is used for electron and ion density distribution. The diffusive equilibrium model is similar to that used by Bortnik et al. (2011) except for the different values of the base point R_b, the base density N_b, and the temperature of the ionosphere T_{de}. The three values, $R_b = R_E + 660$ km (660 km is the orbital altitude of DEMETER), $N_b = 2 \times 10^3$ cm^{-3} (at base point) and $T_{de} = 4000$°K (DEMETER's location) are chosen to ensure the electron temperature and number density matches DEMETER's measurement of electron temperature = 4000°K and density = 1.5×10^4 cm^{-3} (recorded by the Langmuir probe, not shown) in the upper ionosphere. The electron density distribution, computed from the diffusive equilibrium model (Bortnik et al., 2011), is shown as background with gray color scales in Figure 6. The dipole field lines for L = 1.2, 1.4, 1.6, 1.8, and 2.0 are denoted with black dashed lines.

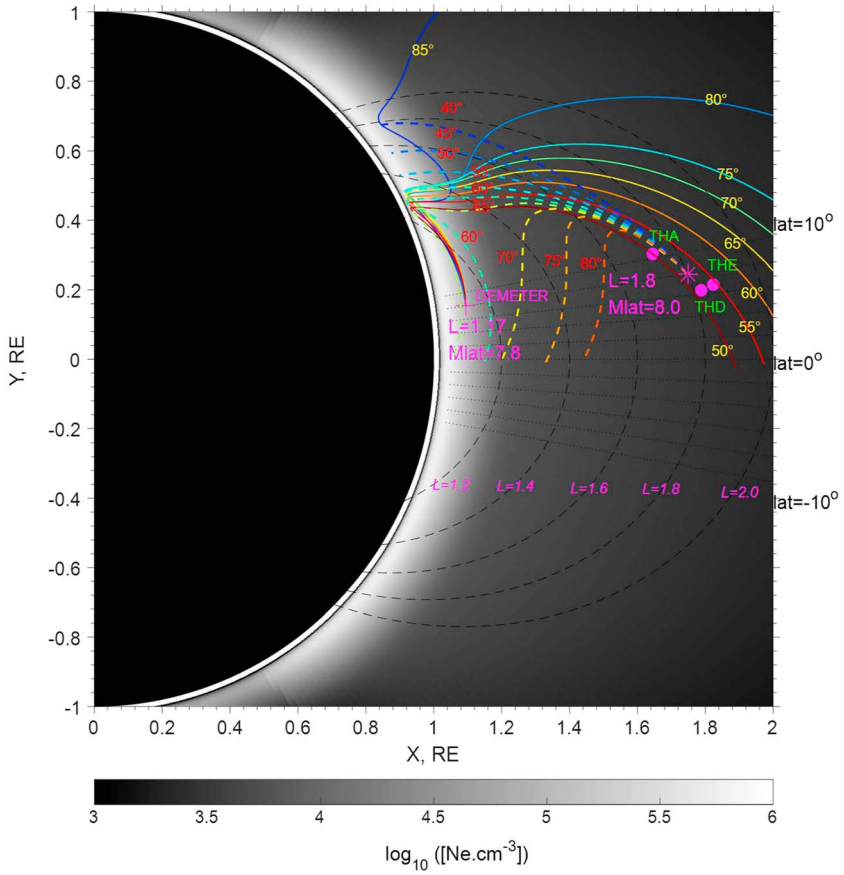

Figure 6. Backward ray tracing simulation from DEMETER and forward ray tracing simulation from THEMIS. The simulation was made for a fixed frequency of 500 Hz over a range of initial wave normal angles: Backward ray tracing from 40° to 80° and forward ray tracing from 50° to 85° both in 5° increments. The solid colored lines represent backward rays launched at DEMETER's location (MLAT = 7.8 and L = 1.17), and colored dashed lines denote forward rays launched at THEMIS's location (MLAT = 8.0 and L = 1.8). Black dashed lines represent L shell, and background color (gray) represents the distribution of plasma density.

Using medium conditions based on the above observations, we performed forward ray tracing from the THEMIS locations and a backward ray tracing launched from DEMETER's location, to examine whether the connection of hiss emissions between the two remote locations is physically possible through wave propagation. We adopted locations of satellites at 14:56:45 UT as the input parameters for the simulation model. At this time, DEMETER locates at MLAT ~7.8° and L shell ~1.17, THA probe locates at ~10.42° and L shell ~1.73, THD at MLAT ~6.35° and L shell ~1.82, and THE at MLAT ~6.69° and L value 1.86. Therefore, we set THEMIS's location at MLAT = 8.0° and L = 1.8 in the simulation. The frequency for ray tracing is set to 500 Hz according to the observed peak frequency of both the ionospheric and plasmaspheric hiss. The ray tracing results are presented in Figure 6.

The colored dashed lines in Figure 6 represent the raypaths of plasmaspheric hiss with a fixed frequency of 500 Hz, which are launched from THEMIS location (MLAT = ~8.0°, L = 1.8, marked by the magenta asteroid symbol) and propagate forward in time from the inner magnetosphere to the upper ionosphere. An array of initial wave normal angles from 40° to 80° at a spacing of 5° was adopted and denoted by different colors. We choose a range of wave normal angles because there is no burst mode waveform from THEMIS probes to extract wave propagation parameters. The exact positions of THA, THD, and THE are denoted by magenta solid dots. It can be seen from the colored dashed lines that when the oblique emissions in the inner magnetosphere propagates forward from the equatorial region toward to the high-latitude regions, some rays with initial wave normal angles over 70° reflect inside the plasmasphere, while other rays with initial wave normal angles below 70° can access the ionosphere and subsequently reflect toward the location of DEMETER (MLAT = 7.8, L = 1.17, marked by the magenta cross symbol).

The colored solid lines in Figure 6 denote the raypaths of ionospheric hiss launched from the DEMETER location with a fixed frequency of 500 Hz. We perform the backward ray tracing with an array of initial wave normal angles from 50° to 85° at a spacing of 5° according to the above statistical distribution of wave propagation parameters (Figure 4e). It can be seen from the colored solid lines that oblique emissions with initial wave normal angles 50° to 70° launched at DEMETER location can be traced back to the THEMIS location. Evidently, both the backward ray tracing simulation and forward ray tracing simulation indicate that the link between two hiss emissions at remote locations is physically possible through wave propagation.

In all, both the conjugate observations and ray tracing simulations suggest that the downward plasmaspheric hiss is indeed a generation source of ionospheric hiss. The generation mechanism of ionospheric hiss is a challenging issue due to the complicated atmosphere-ionosphere-magnetosphere system. Except for the downward magnetospheric emission (e.g., Bortnik et al., 2008, Chen et al., 2017, and reference therein), the lightning activities from the atmosphere also serve as another embryonic source (Green et al., 2005; Meredith, Horne, Clilverd, et al., 2006; Santolík et al., 2009). In Figures 2a and 2b, the intense emissions at 14:50 to 14:54 UT show a series of burst spectra as vertical lines over the whole frequency range are induced by lightning activities. The statistical distribution of wave propagation parameters (not shown) at 14:50 to 14:54 UT shows that azimuthal angles of wave vector and Poynting flux predominate around 0°, suggesting that these lighting induced emissions propagate away from the Earth to the increasing *L* shell direction with a small wave normal angle (mainly 40°–50°). However, Thorne et al. (2006) suggest that the lightning cannot account for hiss over the main frequency range (0.1–2 kHz), for the reason that lightning induced hiss is mainly linked to the plasmaspheric hiss above 2 kHz. In addition to the above mentioned two embryonic sources, the contribution of local growth in plasmasphere (e.g., Chen et al., 2014; Omura et al., 2015) also should be taken into consideration for the mechanism of hiss generation. We leave these generation mechanisms for more comprehensive studies in future.

5. Conclusions

On 15 June 2010, the low Earth orbit satellite DEMETER and the high-altitude elliptical orbit spacecraft THEMIS simultaneously captured the extremely low frequency hiss waves at conjugate positions from 14:51:10 to 15:12:00 UT, when DEMETER was passing through the *L* shell range ~1.39 to 2.8 at a low altitude of 660 km, and the three THEMIS probes were closely flying across the *L* shell range from ~1.64 to 1.91 at altitudes from 1.6 to 2.0 R_E.

The ionospheric hiss recorded by DEMETER appears as a narrowband spectra over a frequency range from 350 to 800 Hz, propagating obliquely (with wave normal angles ranging from 50° to 85°) downward to the Earth and slightly toward the equatorial region with right-handed polarizaiton. The plasmaspheric hiss captured by THEMIS probes in the inner magnetosphere mainly appears over a frequency range from 350 to 900 Hz. Our analyses indicate that these two emissions share similar time-frequency structures and spectral properties. The ray tracing simulations with constraint of the conjugate observations confirm that the link between two hiss emissions at remote locations is physically possible through wave propagation. Prior to this study, there have been no multiple-point observations to directly reveal the relationship between the ionospheric and plasmaspheric hiss.

Acknowledgments
We acknowledge DEMETER scientific mission center for providing observations of electromagnetic field and ionospheric plasma parameters (IMSC, ICE, and ISL) and NASA Goddard Space Flight Center Space Physics Data Facility (http://cdaweb.gsfc.nasa.gov/istp_public/) for the data of the THEMIS spacecraft (FGM, SCM, EFI, and ESA). This work was supported by the NSFC grants 41574139, 41204136, and 41674164; ISTCP 2014DFR21280, the APSCO-SP/PM-EARTHQUAKE Project and ISSI-BJ project, and the Fundamental Research Funds for earthquake research 2014IES010203. Lunjin Chen acknowledges the support of NSF grant AGS 1405041.

References

Angelopoulos, V. (2008). The THEMIS mission. *Space Science Reviews*, *141*, 5–34. https://doi.org/10.1007/s11214-008-9336-1

Auster, H., Glassmeier, K. H., Magnes, W., Aydogar, O., Baumjohann, W., Constantinescu, D., … Wiedemann, M. (2008). The THEMIS fluxgate magnetometer. *Space Science Reviews*, *141*, 235–264. https://doi.org/10.1007/s11214-008-9365-9

Berthelier, J., Godefroy, M., Leblanc, F., Malingre, M., Menvielle, M., Lagoutte, D., … Pfaffe, R. (2006). ICE, the electric field experiment on DEMETER. *Planetary and Space Science*, *54*, 456–471. https://doi.org/10.1016/j.pss.2005.10.016

Bonnell, J., Mozer, F. S., Delory, G. T., Hull, A. J., Ergun, R. E., Cully, C. M., … Harvey, P. R. (2008). The Electric Field Instrument (EFI) for THEMIS. *Space Science Reviews*, *141*, 303–341. https://doi.org/10.1007/s11214-008-9469-2

Bortnik, J., Chen, L., Li, W., Thorne, R. M., & Horne, R. B. (2011). Modeling the evolution of chorus waves into plasmaspheric hiss. *Journal of Geophysical Research*, *116*, A08221. https://doi.org/10.1029/2011JA016499

Bortnik, J., Li, W., Thorne, R. M., Angelopoulos, V., Cully, C., Bonnell, J., … Roux, A. (2009). An observation linking the origin of plasmaspheric hiss to discrete chorus emissions. *Science*, *324*, 775–778. https://doi.org/10.1126/science.1171273

Bortnik, J., Thorne, R. M., & Meredith, N. P. (2008). The unexpected origin of plasmaspheric hiss from discrete chorus emissions. *Nature*, *452*, 62–66. https://doi.org/10.1038/nature06741

Breneman, A., Halford, A., Millan, R., McCarthy, M., Fennell, J., Sample, J., … Kletzing, C. A. (2015). Global-scale coherence modulation of radiation-belt electron loss from plasmaspheric hiss. *Nature*, *523*(7559), 193–195. https://doi.org/10.1038/nature14515

Chen, L., Bortnik, J., Li, W., Thorne, R. M., & Horne, R. B. (2012). Modeling the properties of plasmaspheric hiss: 1. Dependence on chorus wave emission. *Journal of Geophysical Research*, *117*, A05202. https://doi.org/10.1029/2011JA017201

Chen, L., Santolík, O., Hajoš, M., Zheng, L., Zhima, Z., Heelis, R., … Parrot, M. (2017). Source of the low-altitude hiss in the ionosphere. *Geophysical Research Letters*, *44*, 2060–2069. https://doi.org/10.1002/2016GL072181

Chen, L., Thorne, R. M., Bortnik, J., Li, W., Horne, R. B., Reeves, G. D., … Fennell, J. F. (2014). Generation of unusually low frequency plasmaspheric hiss. *Geophysical Research Letters*, *41*, 5702–5709. https://doi.org/10.1002/2014GL060628

Chen, L., Thorne, R. M., Li, W., Bortnik, J., Turner, D., & Angelopoulos, V. (2012). Modulation of plasmaspheric hiss intensity by thermal plasma density structure. *Geophysical Research Letters*, *39*, L14103. https://doi.org/10.1029/2012GL052308

Fu, H. S., Tu, J., Cao, J. B., Song, P., Reinisch, B. W., Gallagher, D. L., & Yang, B. (2010). IMAGE and DMSP observations of a density trough inside the plasmasphere. *Journal of Geophysical Research*, *115*, A07227. https://doi.org/10.1029/2009JA015104

Green, J. L., Boardsen, S., Garcia, L., Taylor, W. W. L., Fung, S. F., & Reinisch, B. W. (2005). On the origin of whistler mode radiation in the plasmasphere. *Journal of Geophysical Research*, *110*, A03201. https://doi.org/10.1029/2004JA010495

Hayosh, M., Pasmanik, D. L., Demekhov, A. G., Santolik, O., Parrot, M., & Titova, E. E. (2013). Simultaneous observations of quasi-periodic ELF/VLF wave emissions and electron precipitation by DEMETER satellite: A case study. *Journal of Geophysical Research*, *118*, 4523–4533. https://doi.org/10.1002/jgra.50179

Horne, R. (1989). Path-integrated growth of electrostatic waves: The generation of terrestrial myriametric radiation. *Journal of Geophysical Research*, *94*(A7), 8895–8909. https://doi.org/10.1029/JA094iA07p08895

Lebreton, J.-P., Stverak, S., & Travnicek, P. (2006). The ISL Langmuir probe experiment processing onboard DEMETER: Scientific objectives, description and first results. *Planetary and Space Science*, *54*, 472–486. https://doi.org/10.1016/j.pss.2005.10.017

McFadden, J., Carlson, C. W., Larson, D., & Angelopolos, V. (2008). THEMIS ESA first science results and performance issues. *Space Science Reviews*, *141*(1-4), 477–508. https://doi.org/10.1007/s11214-008-9433-1

Meredith, N. P., Horne, R. B., Clilverd, M. A., Horsfall, D., Thorne, R. M., & Anderson, R. R. (2006). Origins of plasmaspheric hiss. *Journal of Geophysical Research*, *111*, A09217. https://doi.org/10.1029/2006JA011707

Meredith, N. P., Horne, R. B., Glauert, S. A., Thorne, R. M., Summers, D., Albert, J. M., & Anderson, R. R. (2006). Energetic outer zone electron loss timescales during low geomagnetic activity. *Journal of Geophysical Research*, *111*, A05212. https://doi.org/10.1029/2005JA011516

Němec, F., Santolík, O., Parrot, M., Pickett, J. S., Hayosh, M., & Cornilleau-Wehrlin, N. (2013). Conjugate observations of quasi-periodic emissions by cluster and DEMETER spacecraft. *Journal of Geophysical Research*, *118*, 198–208. https://doi.org/10.1029/2012JA018380

Omura, Y., Nakamura, S., Kletzing, C. A., Summers, D., & Hikishim, M. (2015). Nonlinear wave growth theory of coherent hiss emissions in the plasmasphere. *Journal of Geophysical Research*, *120*, 7642–7657. https://doi.org/10.1002/2015JA021520

Parrot, M., Benoist, D., Berthelier, J. J., Błęcki, J., Chapuis, Y., Colin, F., … Zamora, P. (2006). The magnetic field experiment IMSC and its data processing onboard DEMETER: Scientific objectives, description and first results. *Planetary and Space Science*, *54*, 441–455. https://doi.org/10.1016/j.pss.2005.10.015

Parrot, M., Buzzi, A., SantolíK, O., Berthelier, J. J., Sauvaud, J. A., & Lebreton, J. P. (2006). New observations of electromagnetic harmonic ELF emissions in the ionosphere by the DEMETER satellite during large magnetic storms. *Journal of Geophysical Research*, *111*, A08301. https://doi.org/10.1029/2005JA011583

Parrot, M., Němec, F., & Santolík, O. (2014). Analysis of fine ELF wave structures observed poleward from the ionospheric trough by the low-altitude satellite DEMETER. *Journal of Geophysical Research*, *119*, 2052–2060. https://doi.org/10.1002/2013JA019557

Parrot, M., Santolík, O., & Němec, F. (2016). Chorus and chorus-like emissions seen by the ionospheric satellite DEMETER. *Journal of Geophysical Research*, *121*, 3781–3792. https://doi.org/10.1002/2015JA022286

Roux, A. H., Le Contel, O., Coillot, C., Bouabdellah, A., de la Porte, B., Alison, D., … Vassal, M. C. (2008). The search coil magnetometer for THEMIS. *Space Science Reviews*, *141*, 265–275. https://doi.org/10.1007/s11214-008-9455-8

Rudemo, M. (1982). Empirical choice of histograms and kernel density estimators. *Scandinavian Journal of Statistics*, 65–78.

Santolík, O., Chum, J., Parrot, M., Gurnett, D. A., Pickett, J. S., & Cornilleau-Wehrlin, N. (2006). Propagation of whistler mode chorus to low altitudes: Spacecraft observations of structured ELF hiss. *Journal of Geophysical Research*, *111*, A10208. https://doi.org/10.1029/2005JA011462

Santolík, O., Němec, F., Parrot, M., Lagoutte, D., Madrias, L., & Berthelier, J. J. (2006). Analysis methods for multi-component wave measurements on board the DEMETER spacecraft. *Planetary and Space Science*, *54*, 512–527. https://doi.org/10.1016/j.pss.2005.10.020

Santolík, O., Parrot, M., Inan, U. S., Burešová, D., Gurnett, D. A., & Chum, J. (2009). Propagation of unducted whistlers from their source lightning: A case study. *Journal of Geophysical Research*, *114*, A03212. https://doi.org/10.1029/2008JA013776

Santolík, O., Parrot, M., & Lefeuvre, F. (2003). Singular value decomposition methods for wave propagation analysis, *Radio Science*, *38*(1), 1010. https://doi.org/10.1029/2000RS002523.

Sonnerup, B. U., & Scheible, Ö. M. (1998). In G. Paschmann & P. W. Daly (Eds.), *Minimum and maximum variance analysis, Analysis methods for multi-spacecraft data*. Bern: ISSI.

Thorne, R. M. (2010). Radiation belt dynamics: The importance of wave-particle interactions. *Geophysical Research Letters*, *37*, L22107. https://doi.org/10.1029/2010GL044990

Thorne, R. M., Boardsen, S., Garcia, L., Fung, S. F., & Reinisch, B. W. (2006). Comment on "On the origin of whistler mode radiation in the plasmasphere" by Green et al. *Journal of Geophysical Research*, *111*, A09210. https://doi.org/10.1029/2005JA011477

Thorne, R. M., Smith, E. J., Burton, R. K., & Holzer, R. E. (1973). Plasmaspheric hiss. *Journal of Geophysical Research*, *78*(10), 1581–1596. https://doi.org/10.1029/JA078i010p01581

Tsyganenko, N. A., & Stern, D. P. (1996). Modeling the global magnetic field of the large-scale Birkeland current systems. *Journal of Geophysical Research*, *101*(A12), 27187–27198. https://doi.org/10.1029/96JA02735

Zhima, Z., Cao, J., Liu, W., Fu, H., Yang, J., Zhang, X., & Shen, X. (2013). DEMETER observations of high-latitude chorus waves penetrating the plasmasphere during a geomagnetic storm. *Geophysical Research Letters*, *40*, 5827–5832. https://doi.org/10.1002/2013GL058089

Zhima, Z., Cao, J. B., Liu, W. L., Fu, H. S., Wang, T. Y., Zhang, X. M., & Shen, X. H. (2014). Storm time evolution of ELF/VLF waves observed by DEMETER satellite. *Journal of Geophysical Research: Space Physics*, *119*, 2612–2622. https://doi.org/10.1002/2013JA019237